Article

Droplet-Based Microfluidic Platform for High Spatiotemporal Resolved Single-Cell Signaling Profiling

Yingnan Sun [1],*, Qingqing Tian [1], Yongshu Liu [1], Kunming Xing [2], Yuyan Li [1], Yumin Liu [1] and Shusheng Zhang [1],*

1 Shandong Province Key Laboratory of Detection Technology for Tumor Makers, School of Medicine, Linyi University, Linyi 276005, China
2 Linyi People's Hospital, Linyi 276100, China
* Correspondence: syingnan@126.com (Y.S.); shushzhang@126.com or zhangshusheng@lyu.edu.cn (S.Z.)

Abstract: A small indentation embedded in a microchannel creates a surface energy well (SEW) for a confined droplet due to surface energy release. Inspired by this, we developed a SEW-based microfluidic platform to realize high spatiotemporal-resolved signal profiling at the single-cell level applying droplet stimulus on a single chip. The method allows for controlled droplet replacement within only 3 s with almost 100% exchange efficiency, reliable single-cell patterning of adherent cells and successive treatment of adherent cells with reagent droplets. Furthermore, the PDGFR/Akt pathway served as a model system for evaluating the performance of the SEW-based method in determining the effects of ligand stimulation duration (3 s to 3 min) on receptor phosphorylation. The novel strategy offers a general platform for probing the temporal dynamics of single cells, as well for monitoring rapid chemical reactions in various applications.

Keywords: droplet microfluidics; single cells; cell signaling profiling; high spatiotemporal resolution

1. Introduction

Because the majority of important cellular processes involved in proliferation, differentiation and reprogramming are transient in nature, functional temporal analysis with high temporal resolution is being increasingly sought in research on signaling events involving networks of diverse biochemical reactions that lead to diverse cellular responses depending on stimulus duration [1–3]. Furthermore, because cells are highly heterogeneous and dynamic in response to stimulus perturbation, single-cell analysis would contribute significantly to advancing cancer research, since a drug targeted for one tumor cell phenotype is not necessarily effective against other phenotypes [4–8]. The current, well-established individual cellular analysis technologies involve dissociation and isolation procedures, which can be roughly classified as flow/mass cytometry [9–11], and microfluidics-based techniques [12–14]. However, a drawback of these methods is the inability to probe single-cell events while retaining the adherent cell phenotype in situ with sufficient temporal or spatial resolution required for characterizing the fast kinetics of cellular events [15–19]. Hence, robust temporal profiling of single-cell dynamics while retaining cellular spatial configuration remains challenging for the majority of available techniques.

To overcome these limitations, several technologies have been successfully developed. These bridge the divide between temporal profiling of single cells with precise spatial confinement and the phenotype of adherent cells, and achieve flow confinement within a living cell. Specifically, these technologies can be broadly classified as flow-based microfluidics comprising individual addressable cell culture chambers [20], digital microfluidics with electrode arrays for droplet manipulation [21], nanopipettes with asymmetric nanopore electrodes for current amplification [22,23], atomic force microscopy (AFM) tips with microchannels for force flow confinement [24,25] and micropipettes with electrodes for hydrodynamic flow confinement [15,26]. All of these methods allow for the perturbation

and analysis of single adherent cells with high temporal resolution and controlled spatial precision, an important property that is lacking in most analytical systems. Despite the fact that the new detection strategies based on these platforms enable the acquisition of detailed information on single cells with high spatial and temporal resolution, the fabrication and assembly of extremely fine probes and auxiliary components for observation and control remain challenging because of the stringent requirements for the construction process and operational complexity. Furthermore, with the exception of microfluidics, other in-situ technologies are not well suited for applications such as extracellular excitation and imaging analysis, and their throughput is limited by the device complexity, configuration and end-point detection mode. Therefore, the ability to perform multiple manipulation procedures on living adherent cells with high spatiotemporal resolution at the single-cell level remains limited.

An alternative droplet-based microfluidics system embedded with indentations in a wide and low channel has been previously reported for sequential droplet manipulation, including trapping and replacement, based on modulating droplet confinement [27,28]. Because the indentations are beneficial for surface energy release and capable of holding droplets locally, herein they are referred to as "surface energy wells" (SEWs), in analogy with particle trapping in potential energy wells, which have also been termed Hele-Shaw cells or anchors in other studies [29,30]. This finding inspired us to explore whether the SEW structure can be utilized to achieve rapid droplet replacement over living cells for rapid biochemical reaction monitoring. To date, only one study has been reported on the application of a SEW-based device on long-term cell culturing and controlled stimulation, wherein adherent cells were confined within a gelation scaffold to resist the flush of liquid flow and maintain in situ growth while various reagents were successively introduced [31]. Although this platform is capable of monitoring cell death dynamics upon various drug exposure regimes, a low time resolution of several minutes compromised its quantification performance.

In this study, we extended the SEW-based droplet microfluidics approach to achieve high spatiotemporal resolution for in situ single-cell signal profiling on a single chip, by leveraging the SEW structure for droplet manipulation and single-cell patterning. To the best of our knowledge, this study is the first comprehensive evaluation of the temporal resolution and exchange efficiency of a chip entailing the SEW structure. Furthermore, in comparison to the above-mentioned study [31], the SEW chip was designed and optimized for achieving living adherent single-cell patterning without resorting to hydrogel scaffolds, as well as for tracing the rapid dynamics of protein phosphorylation events whose unfolding is typically in the order of seconds.

The specific achievements of this study include the following: (1) A microfluidic chip comprising dual inlets and a SEW array are controlled by varying only the flow rate of the carrier oil. (2) Droplet replacement was evaluated as rapidly as 3 s and the content exchange efficiency reached 100%, indicating that complete termination of the original stimulus can be achieved with a single droplet replacement. (3) Adherent cells were cultured on the floor of the chamber under continuous medium perfusion, and single-cell cultures were achieved by harnessing the hydrodynamic flow variations in the SEW region. (4) The well-established PDGFR/Akt pathway was chosen as a model system of fast cellular events to monitor the dynamics of receptor phosphorylation in response to a cell stimulus with a time resolution of seconds. Therefore, we propose that this method can potentially be applied as an important new strategy for probing the temporal dynamics of fast cellular events at the single-cell level in a wide range of applications.

2. Materials and Methods

2.1. Device Fabrication and Assembly

The materials for microfluidic device fabrication included an SU-8 2035 positive photoresist (Microchem, Westborough, MA, USA), Si wafers (Shuguang, Tianjin, China), and a polydimethylsiloxane elastomer kit (PDMS, Sylgard 184, Dow Corning). All tubing

and fittings were acquired from Suzhou CChip. An SU-8 model with two patterns of equal depth (35 μm high) was prepared employing soft photolithography on a silicon wafer. Next, a PDMS layer was obtained by casting the PDMS precursor (base to curing agent weight ratio of 10:1) onto the prepared SU-8 mold, followed by curing for 30 min at 85 °C. Then, the cured PDMS layer was gently peeled off the mold to obtain a PDMS-negative mode structure, followed by cutting into two parts along the borders, that is, the top and bottom layers of the chip. The top layer comprised inlets, an outlet and an SEW array, and the bottom layer contained fluidic channels for aqueous media and oil flow. After creating the inlets and outlet in the top layer, the cross marks were aligned accordingly and the two layers were bonded after 90 s of plasma treatment in the high-power mode (Harrick PDC-002). In the final step, the chip was connected to the pressure pumps by tubing and fittings for medium perfusion.

2.2. Surface Modification

For the chip to allow for both stable droplet generation and adherent cell growth, two types of surface treatments were applied on separate sections of the internal microchannels. (1) For the droplet generation section: to render the internal channel surface hydrophobic, a dilute solution of 1H1H2H2H-perfluorodecyltrichlorosilane (Sigma-Aldrich) in FC40 oil (3M Fluorinert) (1% v/v, 10 μL) was injected via the inlet to fill the generation section without entering the downstream trapping chamber. The chip was maintained at 20 °C for approximately 20 min and then rinsed twice with pure FC40 to remove residual chemicals and deliver a hydrophobic PDMS surface. (2) For the trapping chamber: to further accelerate cell adhesion from the suspension onto the bottom of the chamber, a fibronectin solution (15 μg/mL, 350 μL) (Solarbio, Beijing, China) was perfused into the trapping chamber via the outlet without entering the upstream transporting channel [32]. The chip was incubated overnight at 4 °C to allow fibronectin to coat the plasma-treated inner surface. The coating solution was then removed from the chip via suction and the chip was washed twice with PBS via the same outlet using a syringe.

2.3. Cell Culture and Viability

The MCF-7 and 4T1 cell lines used in this study were purchased from Beyotime (Shanghai, China). All cell culture reagents were purchased from Solarbio Science & Technology (Beijing, China), including DMEM, fetal bovine serum (FBS), penicillin/streptomycin (P/S), PBS and Trypsin-EDTA. Hoechst 33342 (Thermo Fisher, Waltham, MA, USA) and fluorescein diacetate (FDA, Sigma-Aldrich, St. Louis, MO, USA) were used as the cell staining reagents The adherent cells were cultured in DMEM containing 100 U/mL P/S supplemented with 10% FBS and maintained at 37 °C in a humidified incubator containing 5% CO_2. Upon reaching 70–80% confluency, the cells were trypsinized and centrifugated, and then resuspended in culture medium for cell seeding onto the chip. Similar to the fibronectin coating operation, the cell suspension (~0.5–1 × 10^6 cells/mL) was injected into the trapping chamber via the outlet without entering the upstream channel. The cells were allowed to settle uniformly and attach slightly for 20 min under static conditions, followed by continuous perfusion of fresh culture medium to ensure nutrient and air supply for the cells in the narrow culture chamber. Importantly, the flow rate was maintained at 1 μL/min for a duration of 2 h. Eventually, the cells were well-attached with visible microvilli, appearing polygonal in shape. Hoechst 33342 (10 μg/mL) and FDA (5 mg/mL) solutions were used in combination to asses cell viability. After incubation for 10 min, the staining solution was removed by gentle washing with fresh growth media and recovered for fluorescence imaging.

2.4. Single-Cell Immunocytochemistry

The cell immunocytochemistry reagents included: (1) fixing solution: 4% paraformaldehyde (Solarbio, No.P1110); (2) blocking buffer: 10% (v/v) normal goat serum (Solarbio, No.SL038) and 0.3% (v/v) TritonX-100 (Sigma-Aldrich, No.T8787) diluted in PBS; (3) pri-

mary antibody for Akt (Thr308): Phospho-Akt (Thr308) Rabbit mAb (CTS, No.13038T); (4) primary antibody for Akt (Ser473): Anti-Akt1 (Phospho-Ser473) rabbit polyclonal antibody (BBI, No.D155022); (5) second antibody staining solution (second-Ab): Alexa Fluor 555-conjugated Goat anti-rabbit IgG (BBI, No.D110070); (6) ligand solution: recombinant human platelet-derived growth factor-BB (PDGF-BB) (BBI, No.C600154).

Before stimulation, cells were pre-cultured with AKT inhibitor VIII in complete medium (2 μM, Beyotime, SF2784) for 1 h. The immunocytochemistry procedure involved ligand stimulation, fixation, permeabilization, blocking, staining and washing. Specifically, ligand and fixing solutions were applied in the form of droplets, while the other liquids were injected sequentially with continuous flow. Unless otherwise stated, droplet operations and immunocytochemistry incubations were performed inside a bench incubator. The general procedure was as follows: (1) Single cells pre-inhibited with AKT inhibitor were stimulated by transported droplets of ligand solution (10 ng/mL in serum-free DMEM); stimulus duration was varied depending on the experiment. (2) Immediately after stimulation, the ligand droplets were replaced by fixing solution droplets to fix the single cells, followed by incubation for 10 min. (3) The fixing droplets were then flushed away with blocking buffer, followed by incubation for 1 h. (4) The blocked cells were stained with primary antibodies by perfusing primary antibody Thr308 solution (1:800 dilution) followed by incubation overnight at 4 °C. (5) The unbound primary antibodies were removed by injecting PBS. (6) The primary antibodies were stained by secondary IgG555 antibodies by injecting secondary antibody solution (1:200 dilution) and incubating for 2 h. Finally, the cells were rinsed twice with PBS.

2.5. Experimental Setup

The entire microfluidic device functioned within a Dolomite microfluidic system (Royston, UK), which was equipped with: (1) a high-speed digital microscope (Meros, 3200531) for capturing high-speed droplet production and replacement with a frame rate of ~4100 fps and an exposure time of 0.05 ms; (2) flow control center software (Basic, Dolomite) for accurate and simultaneous control of Dolomite modules; (3) pressure pumps (Mitos p-pump) with a wide flow rate range (from several nL/min to 1 mL/min) and a precise pressure controller (from 0 to 10 bar) connected to flow sensors to allow for highly stable pulseless liquid flow and instant responses. In addition, the bench incubator (WH-SCI-01, Suzhou Wenhao, Suzhou, China) used for cell loading and culturing was connected to the Dolomite system for continuous infusion and in situ observation. Microscopy images were acquired using an inverted fluorescence microscope (IX73, Olympus, Tokyo, Japan), and the grey values of the fluorescence images were processed and determined using ImageJ software.

3. Results and Discussion

3.1. Chip Design for Single-Cell Stimulus

The SEW-based microfluidic platform described herein was designed to perform droplet manipulation for in situ profiling of single-cell signaling with high spatiotemporal resolution by controlling the oil flow rate. Figure 1 shows a detailed schematic of the implementation principle and images of the device and droplet manipulation. The device comprised of a bottom layer with microchannels and a top layer with an SEW array (Figure 1a). For function partitioning, the device assembly included a generation section with a flow-focusing junction, delivery section with a widened channel and a trapping chamber with SEW structures. With regard to the SEW structure, the adjustment in the height confinement of droplets enables their trapping in the chamber due to surface energy release [24]. For a spherical droplet of constant volume, the surface energy is minimal and increases as the droplet is squashed into a flattened shape because of the droplet's surface energy modulation forced by the reduction of the channel's height. The flattened droplet will then be temporarily trapped by an indentation (a portion in the channel with a larger height) located downstream in the wide and thin channel. Therefore, the indentation can be

named the surface energy well (SEW). Furthermore, droplet manipulation within the SEW includes replacement, parking and passing modes, depending on the hydrodynamic drag force of the carrier oil's flow rate, which is proportional to its mean velocity. Figure 1b shows the replacement mode functioning under an appropriate carrier oil flow rate v_{oil} ($v_1 < v_{oil} < v_2$): droplet A is first trapped by an SEW until droplet B appears, collides with droplet A and replaces it; the process is then repeated with droplet C replacing droplet B. On the other hand, droplets under the SEWs undergo parking ($v_{oil} < v_1$) or passing ($v_{oil} > v_2$) modes (Figure S2). It should be noted that the replacement mode enables high temporal and spatial resolution, which has not been addressed in previous studies. A single substitution of one droplet by another in the carrier oil under the SEWs is extremely rapid, allowing for the instantaneous action of distinct reagent droplets on the same SEW region. Therefore, a series of stimulus droplets can be trapped for a very short time over individual adherent cells located in the corresponding position of an SEW and sequentially replaced with termination droplets to achieve rapid immunocytochemistry at the single-cell level (Figure 1c). The SEW configuration is depicted in Figure 1c: the channel height (H) and indentation depth (h) were set to 35 μm, being considerably smaller than the channel width (W = 1.8 mm) and length (L = 3 mm). A confined droplet with a volume larger than V_1 and V_2 (Figure S3) adopts radius R, which is larger than the height of 35 μm. Furthermore, 200 μm center-to-center spacing between two SEWs allowed for the simultaneous observation of single cells. These dimensions were designed considering both droplet volume and oil velocity to avoid sacrificing cell proliferation for high spatiotemporal resolved droplet manipulation.

The complete device shown in Figure 1d was fabricated by the successive application of SU-8 monolayer photolithography, PDMS casting and plasma-assisted bonding. To further render the surface of the generation section hydrophobic and promote cell adherence in the trapping chamber, fluoroalkylsilane and fibronectin were injected and aspirated via the inlet and outlet to modify the upstream and downstream regions, respectively. During droplet operation (Figure 1b), the device operates within a Dolomite microfluidic system equipped with a high-speed digital microscope and flow control center software (Figure 1e). A bench incubator fitted to the Dolomite system (Figure 1f) provides a suitable environment for cell growth. Furthermore, the carrier oil composition must be optimized with regard to the oil and surfactant type and content to realize stable droplet formation, droplet fusion resistance, biocompatibility and to prevent the oil from acting on adherent cells [33,34]. Herein, HFE 7500 oil containing 2% surfactant was adopted. The experiment commenced with the generation of monodisperse aqueous droplets in carrier oil, followed by their delivery downstream with the oil flow, and finally, their arrival in the trapping chamber to be trapped by the SEW array (Figure 1g).
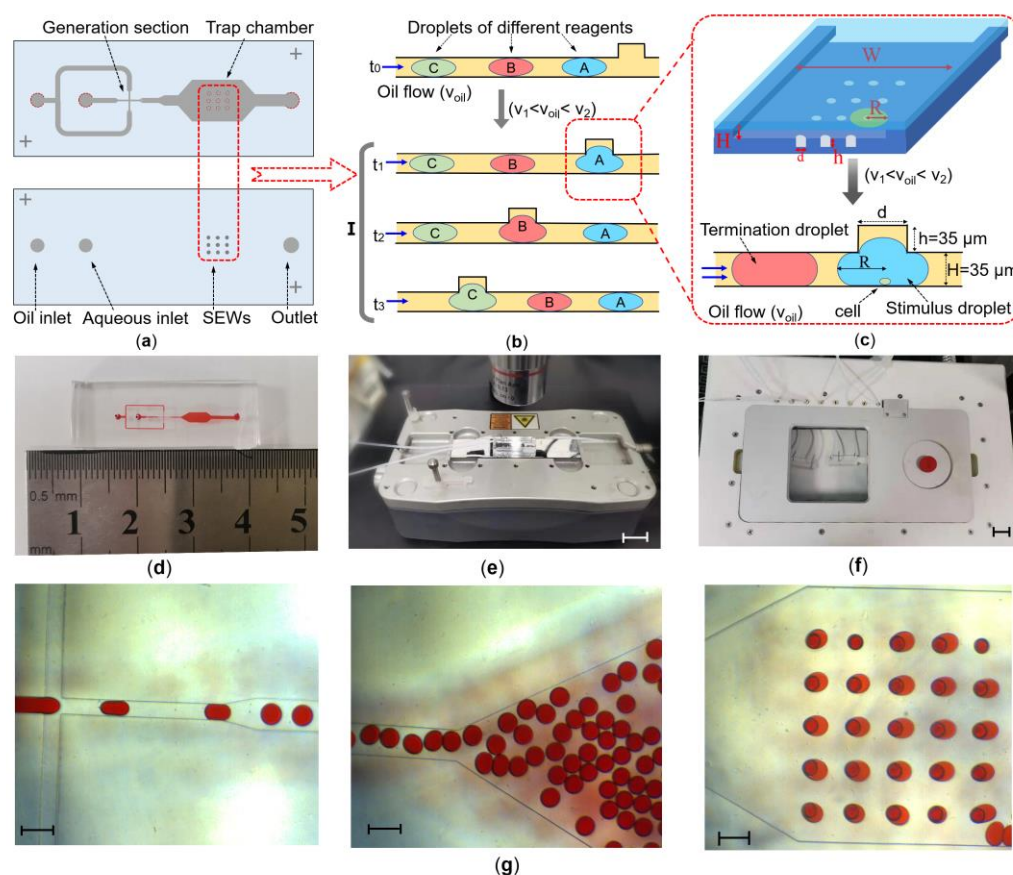
Figure 1. (**a**) Chip design: schematic top view of the microfluidic chip showing the layout of the bottom and top plasma-bonded layers, featuring dual inlets for two-phase flow. The bottom layer comprises the generation section with a flow-focusing junction and a trapping chamber. The top layer is composed of an SEW array, outlet, aqueous liquid and oil inlets for droplet generation and flow rate control. (**b**) Replacement mode: schematic side view of droplets being trapped under the SEW structure due to reduced surface energy. With an increase in the oil flow rate, the trapped droplet (reagent A) is replaced by the oncoming droplet (reagent B), and the sequence is repeated to replace droplet B with droplet C. (**c**) Side-view schematic showing adherent single cells cultured on the bottom layer under the SEWs. The cells were probed for protein phosphorylation with high spatiotemporal control: the ligand droplet (blue) becomes trapped by the SEW, thereby covering the cells for several seconds, followed by replacement by the termination droplet (red). (**d**) Image of the assembled chip filled with red ink. (**e**) Dolomite equipment comprising pressure pumps for microfluidic chip operation and a high-speed digital microscope for observation. (**f**) Bench incubator used for loading cells onto the microfluidic chip and incubation. (**g**) Sequential high-speed microscope images of red ink droplets being generated, delivered to the trapping chamber and trapped (left to right). Scale bars: 200 μm.

3.2. Trapping and Release Performance of the Chip

The dual-inlet configuration enables the simultaneous production of monodisperse droplets with a specific volume, and droplet manipulation through delivery velocity control, both of which are dependent on the oil flow rate. Consequently, the complexity of device operation is reduced. However, a new challenge arises: ensuring a constant volume of upstream droplets when the oil flow rate is changed to manipulate the downstream droplets. Therefore, a feasible solution is provided by synchronously increasing or decreasing the oil and aqueous flow rates within a certain range. As shown in Figure 2a, the droplet diameter is positively correlated with the liquid velocity at a specific oil velocity. Figure 2b shows generated droplets with diameters of 85, 95, 120 and 150 μm as examples, demonstrating

that a roughly constant droplet volume can be achieved by simultaneously adjusting the oil and liquid velocity.
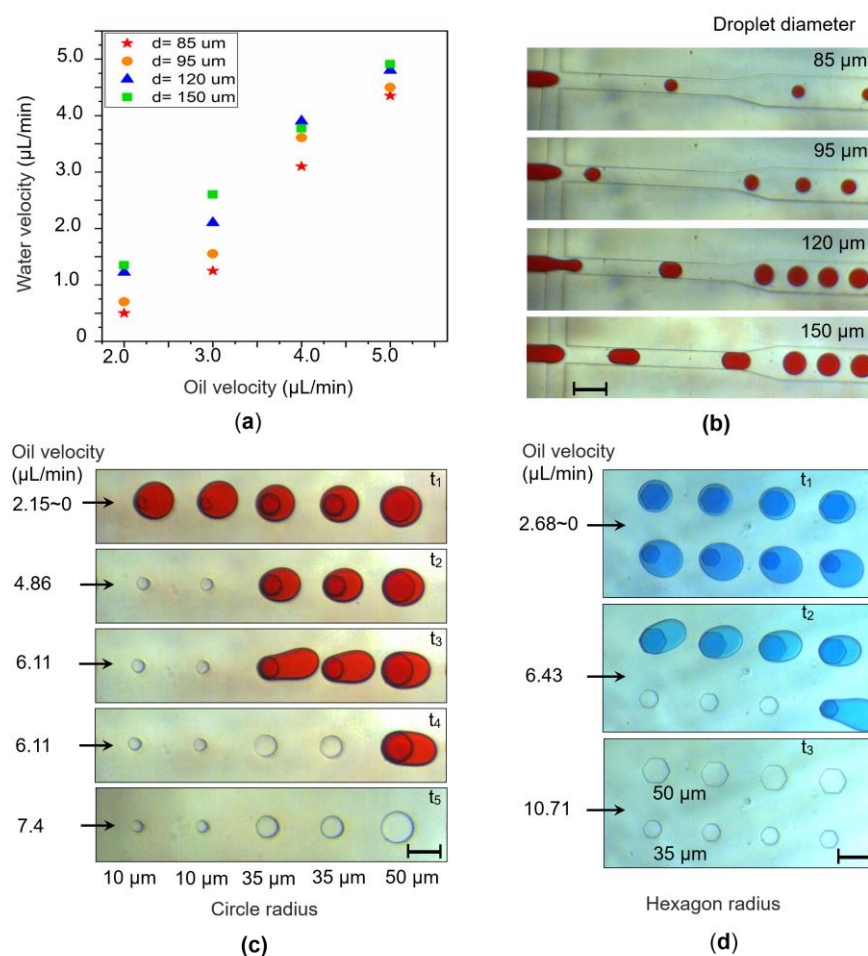

Figure 2. (**a**) The droplet diameter can be kept constant by changing the flow rates of the two phases simultaneously within a certain range, an important prerequisite for the dual-inlet design of the chip. (**b**) High-speed microscopy images of droplets with specific diameters generated by applying varying oil and liquid (red ink) flow rate combinations. Scale bars: 200 μm. (**c**) Circular SEW test: droplets of equal size are pre-trapped by the circular SEWs at a low oil flow rate (t_1). As the oil flow rate gradually increases (t_2~t_5), the trapped droplets are sequentially released, starting from the smallest SEW (10 μm radius), and finally from the largest SEW (50 μm radius). Scale bars: 100 μm. (**d**) The same test was performed using hexagonal SEWs of varying sizes. It was clear that the critical oil rate required for droplet release from the hexagonal SEWs was greater than that from the circular SEWs. Scale bars: 100 μm.

To further determine the optimal oil velocity for cell profiling, SEWs with distinct shapes were adopted to evaluate the corresponding hydrodynamic droplet capture force. Specifically, circular and hexagonal indentations of varying radii were selected as characterization parameters for analyzing droplet trapping and release. As shown in Figure 2c, the droplets were maintained at a volume of roughly 0.8 nL by manipulating the oil and aqueous flow velocities ($v_{aqueous}$ = 2 μL/min, v_{oil} = 2.15 μL/min). Initially, the droplets are instantly captured by all of the circular SEWs and remain in place due to the low oil flow rate. As the carrier oil velocity gradually increases to 7.4 μL/min, the droplets are successively released from SEWs of increasing radius. In addition, the same droplet trapping and release test was performed using hexagonal SEWs with circumradii of 35 and 50 μm. Figure 2d shows that for hexagonal SEWs, the critical release velocity and fluctuations in the release are considerably higher than for the circular holes, which hampers fast and

accurate control of droplet replacement. Taking into account both the oil velocity and fluid shear, the circular SEW with a radius of 50 μm was finally chosen for profiling single-cell signaling to achieve both rapid and stable droplet replacement.

3.3. High-Spatiotemporal Replacement Performance

The developed SEW-based platform is capable of realizing droplet replacement with both high temporal resolution and high content replacement efficiency, which are lacking in most analysis platforms. Herein, we selected the replacement duration time and content exchange ratio as characterization parameters to demonstrate the high spatiotemporal control achieved with the SEW structure. Colored inks were used to aid in the visualization of the rapid process, captured using a high-speed microscope. Figure 3a (top row) shows rapid reagent replacement at a low oil flow rate (v_{oil} = 2.5 μL/min): the black ink droplet is pre-trapped by an SEW, and the colorless PBS droplet is transported by the carrier oil. At frame 46, the PBS droplet makes contact with the black droplet, gradually forcing it out of the SEW until it completely dislodges it at frame 50; finally, the PBS droplet remains parked on the SEW site while the black droplet flows away. Based on a frame rate of 24 fps, one droplet replacement was calculated to be complete within 0.2 s. Furthermore, rapid reagent replacement under a high oil flow rate (v_{oil} = 5.3 μL/min) is shown in Figure 3a (bottom row), applying a frame rate of 96 fps (Figure S4): the red ink droplet replaces the original black ink droplet from under an SEW site and parks there, with a temporal resolution of only 0.04 s. The replacement duration was recorded for varying oil flow rates at 10 positions and a column scatter plot was generated (Figure 3b). Furthermore, the replacement time was determined for a single SEW structure, whereby the dark blue droplet shown in Figure 3c was replaced by the light blue one, which was calculated to be 1.25 s. In all of these cases, the spatial resolution of reagents was the coverage area of a single sub-nanoliter droplet. Therefore, the spatiotemporal resolution of this platform depends on the carrier oil velocity and droplet volume, and it is sufficiently high to enable the rapid single-cell profiling of most transient cellular processes.

An important prerequisite for achieving high temporal resolution is ensuring a high reagent replacement efficiency, ideally with 100% content exchange ratio; this was evaluated based on the residual quantity of fluorescent dyes after droplet replacement. Figure 3d shows the sequential replacement of fluorescent droplets under a 2 × 2 SEW array: red fluorescent droplets (ROX, 50 μg/mL) were initially trapped by the SEWs, and then replaced with green (FN-488, 30 μg/mL), followed by blue (7-Hydroxycoumarin, 25 mg/mL) and finally non-fluorescent (PBS, 1×) droplets under an oil flow rate of 4.2 μL/min. Bright-field and fluorescence images were recorded after each droplet replacement and ImageJ software was used to split the fluorescence channels and determine their corresponding gray values. Figure 3e shows the change in fluorescence with droplet replacement. Two aspects of this histogram are worth noting: (1) At the beginning, the fluorescence image of the ROX droplets exhibited low values in both the blue and green channels. (2) Finally, the fluorescence image of the PBS droplet was obtained under UV excitation and the gray values in all three channels were zero. Hence, the integrated analysis results implied that the gray values of the two channels other than the dye fluorescence channel were neither residual nor background fluorescence, but originated from the intrinsic luminescence spectrum of each fluorescent dye. Accordingly, it can be concluded that single-drop reagent replacement displaces nearly 100% of the original solution under the SEW structure. Notably, such a complete exchange prevents cross contamination from successive stimulation exchanges, and upon replacement with a termination reagent, allows for immediate and complete termination. This feature is crucial for achieving high-time-resolution when monitoring transient biochemical processes, in addition to profiling cell signaling networks.
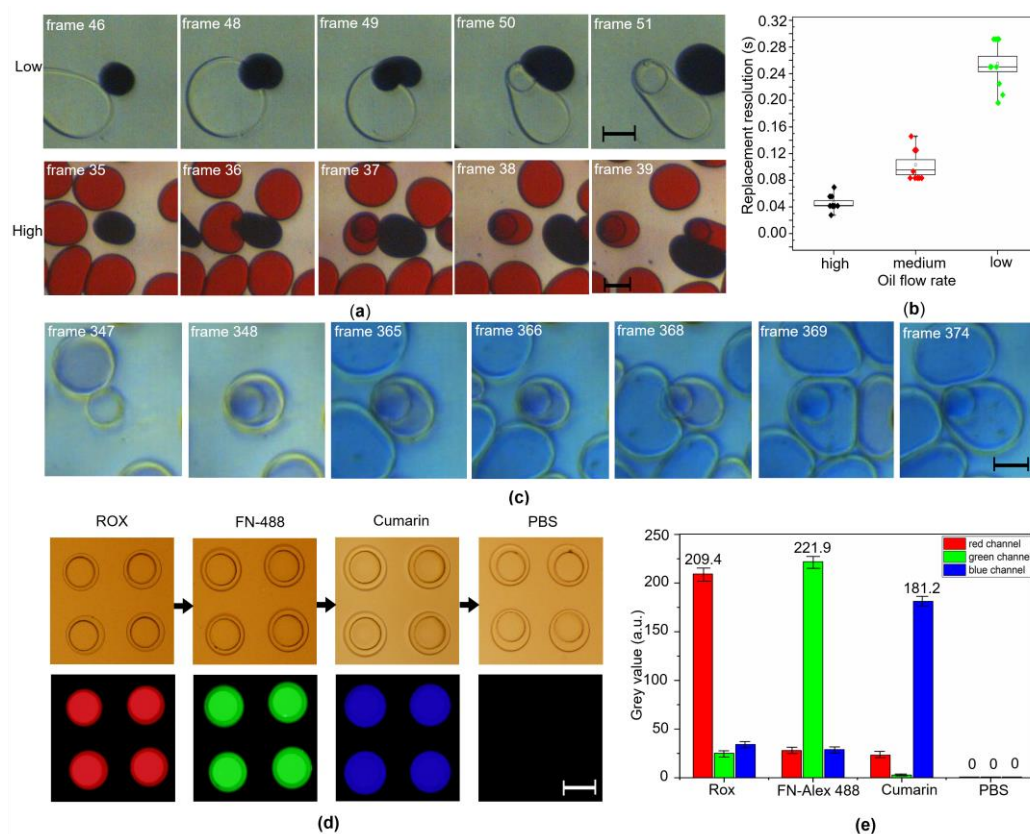
Figure 3. (**a**) Time lapse images of one SEW during the replacement of two aqueous droplets, black to colorless, under a lower oil flow rate (top), and black to red under a higher flow rate (bottom). (**b**) Column scatter plot of the replacement times at 10 positions under varying oil flow rates. (**c**) Time lapse images of droplet replacement (dark blue by light blue) for a single SEW structure. (**d**) Sequential replacement of differently colored droplets under an SEWs array (2 × 2). The top and bottom rows are the bright-field and corresponding fluorescence images, respectively. At the appropriate oil flow rate, ROX droplets are initially trapped under the SEWs, followed by successive replacement with FN-488, 7-Hydroxycoumarin and finally PBS droplets. (**e**) Statistical distribution of the mean gray values of the fluorescence images for three channels, split up and determined using ImageJ software. Scale bars: 100 μm.

3.4. Single Cell Patterning on the Chip

Another crucial step in the high spatiotemporal analysis of cells is obtaining both favorable growth of adherent cells and single-cell patterns that correspond to SEW locations. To achieve this, the cell suspension was loaded into the chamber, followed by the continuous perfusion of fresh culture medium at an extremely slow flow rate to establish a long-term culture of adherent cells in the narrow chamber (Figure S5). After culturing for a period of time, the cells sedimented uniformly and their attachment was promoted by the fibronectin coating (Figure 4a—1). Next, PBS was continuously perfused at a higher flow rate to wash the chamber lightly by removing the residual suspension, and to detach loosely attached cells outside the SEW regions (Figure 4a—2), thereby realizing single-cell patterning corresponding to the SEWs array (Figure 4a—3). The fundamental principle behind the formation of single-cell patterns entails the dissimilar vertical restrictions on transverse liquid flow, arising from the height difference in the narrow channel, which alters the flow velocity in the trapping chamber (Figure 4a). As a result, compared to the SEW region where the channel height was 70 μm, the higher velocity in the region with a height of 35 μm exerts a higher hydrodynamic drag force against the adherent cells, leading to cell detachment. In this study, cell loading and long-term cultivation were performed using a bench incubator with accessibility to medium perfusion and in situ observation. MCF-7 cells with a seeding density ranging from 0.5×10^6 to 1×10^6 cells/mL (100 μL)

were loaded (Figure 4b—t_1) and allowed to adhere loosely on the bottom of the chamber under a culture medium perfusion rate of 1 µL/min (Figure 4b—t_2) to ensure appropriate cell density and cell adhesion strength on the inner surface. After culturing for 3 h, the PBS flow rate was increased to ~10–20 µL/min to obtain a single cell array (Figure 4b—t_3) that corresponded to the SEW array. Culturing was continued for an additional hour to strengthen cell adherence.
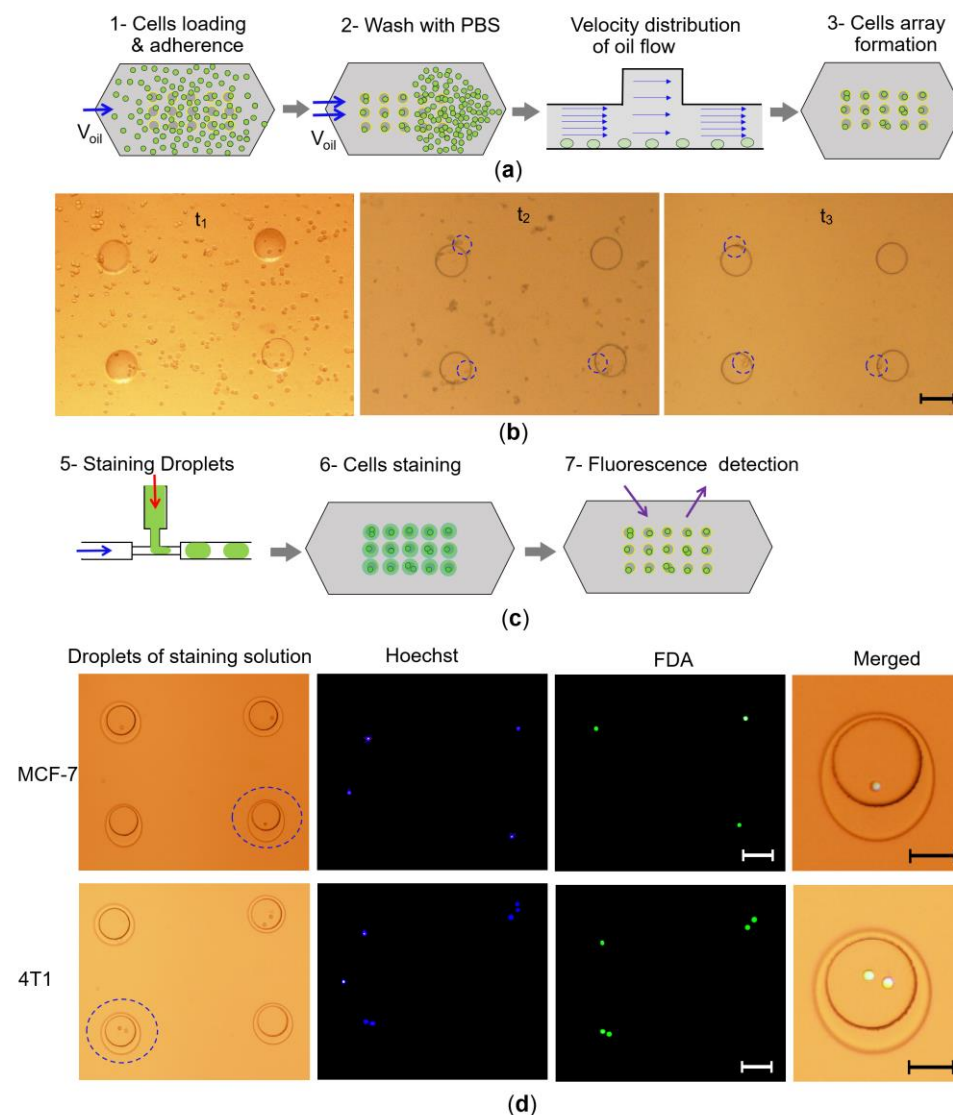

Figure 4. (**a**) Schematic diagram of cell loading, sedimentation, adherence to the bottom of the chamber and growth. Due to the oil flow velocity distribution, with an increasing flow rate of culture medium, single cells are successfully patterned according to the SEW array. (**b**) The bright-field pictures showed the adherence growth of MCF-7 cells on the fibronectin-modified surface. t_1: cell suspension was cultured in the chamber under continuous medium flow. t_2: cells uniformly adhered to the bottom under continuous medium flow at a relatively lower rate for 2 h. t_3: after the culture medium flow rate was increased, single cells appeared in an arrangement corresponding to the cells marked by the dashed blue circles in t_2. Scale bars: 100 µm. (**c**) Schematic diagram for staining single cells by loading various staining droplets; the cells can be viewed directly using a microscope. (**d**) The bright-field and fluorescence images of MCF-7 and 4T1 cell arrays were observed under a 10× objective lens, scale bar: 100 µm, while the merged images (marked by the dashed blue circles in the first column) were observed under larger magnification (20× objective), scale bars: 50 µm. These results provided early information on single cell morphology and viability. Bright droplet = staining solution, blue = cell nuclei (stained by Hoechst) and green = live cells (stained by FDA).

Moreover, to probe the analytical capabilities of the droplet-based method, droplets of cell viability reagents were generated (Figure 4c—5), subsequently trapped by the SEW structures, thereby covering the cells, and then incubated for a certain duration for cell staining (Figure 4c—6), followed by droplet release and fluorescence detection (Figure 4c—7). As shown in Figure 4d, the bright-field photos in the first column indicated that the Hoechst and FDA droplets were trapped by the SEWs on the roof of the chamber, while covering the MCF-7 cells on the bottom. The blue and green fluorescence images, observed under a 20× objective lens, indicated successful nuclear staining and single cell viability of MCF-7. The combined pictures in the right-most column observed under a 40× objective lens, indicated that the single adherent cells maintained their morphological integrity and cell viability for subsequent proliferation. Moreover, to demonstrate the versatility of the new method, 4T1 cells were analyzed in the same manner. The images in Figure 4d show similar single cell patterning under the SEWs with no significant impact on the cell viability. Notably, the successful cell staining using droplets confirmed the feasibility and validity of treating adherent cells with droplets because the SEW structure enables droplet manipulation (Figure S6).

3.5. Single Cell Immunocytochemistry on the Chip

Having established that the SEW-based microfluidics system allows for droplet replacement with high spatiotemporal resolution and adherent cell staining with reagent droplets, we chose the well-characterized PDGFR/PI3K/Akt pathway as a model system to evaluate the performance of the SEW-based method for investigating fast cell signaling events [35–37]. The diagram in Figure 5a illustrates signal transduction in the PDGFR/PI3K/Akt pathway: when the ligand (PDGF) binds to the receptor (PDGFR), the tyrosine of the latter is phosphorylated, serving as a binding site for phosphoinositide 3-kinase (PI-3K). PtdIns(3,4,5)P3 (PIP3) is then generated in response to PI-3K activation, recruiting Akt to the plasma membrane and leading to Akt phosphorylation; these processes have emerged as key regulators of downstream cellular processes [38]. In this experiment, two Akt serine phosphorylation sites involving Ser473 and Thr308 were probed both in MCF-7 and 4T1 cells to evaluate the time-dependent effects of cellular stimuli [39].

Because Akt inhibition can block Akt activation in a concentration-dependent manner [21], at the beginning of on-chip cell preparation, the culture medium was supplemented with 2 μM AKT inhibitor VIII for 3 h to temporarily block the PI3K/Akt pathways in tumor cells. Subsequently, phosphorylation of these inhibited cells was determined as described in the Section 2.5 and schematically depicted in Figure 5b. It is worth mentioning that stimulation and termination in the first two steps were performed using droplets to treat localized cells after trapping, while the subsequent steps entailed solution perfusion. First, under HFE oil (0.8 μL/min) and PDGF-BB solution (0.5 μL/min) flow, the ligand droplets were generated and transported to the chamber at a relatively low speed and then parked there separately for 0, 3 s, 5 s, 10 s and 3 min, then immediately replaced by fixation droplets formed from HFE and formalin flow at rates of 2.2 μL/min and 1.7 μL/min followed by 10 min of incubation. Subsequently, blocking solution (BSA), primary antibody for phospho-Akt (Thr308) and secondary antibody (IgG-Alexa Fluor 555) were sequentially perfused into the chamber for immunocytochemistry reagent exchange, rinsing with PBS at each interval. Finally, the influence of stimulation time on the phosphorylation level was determined based on the fluorescence of individual cells.
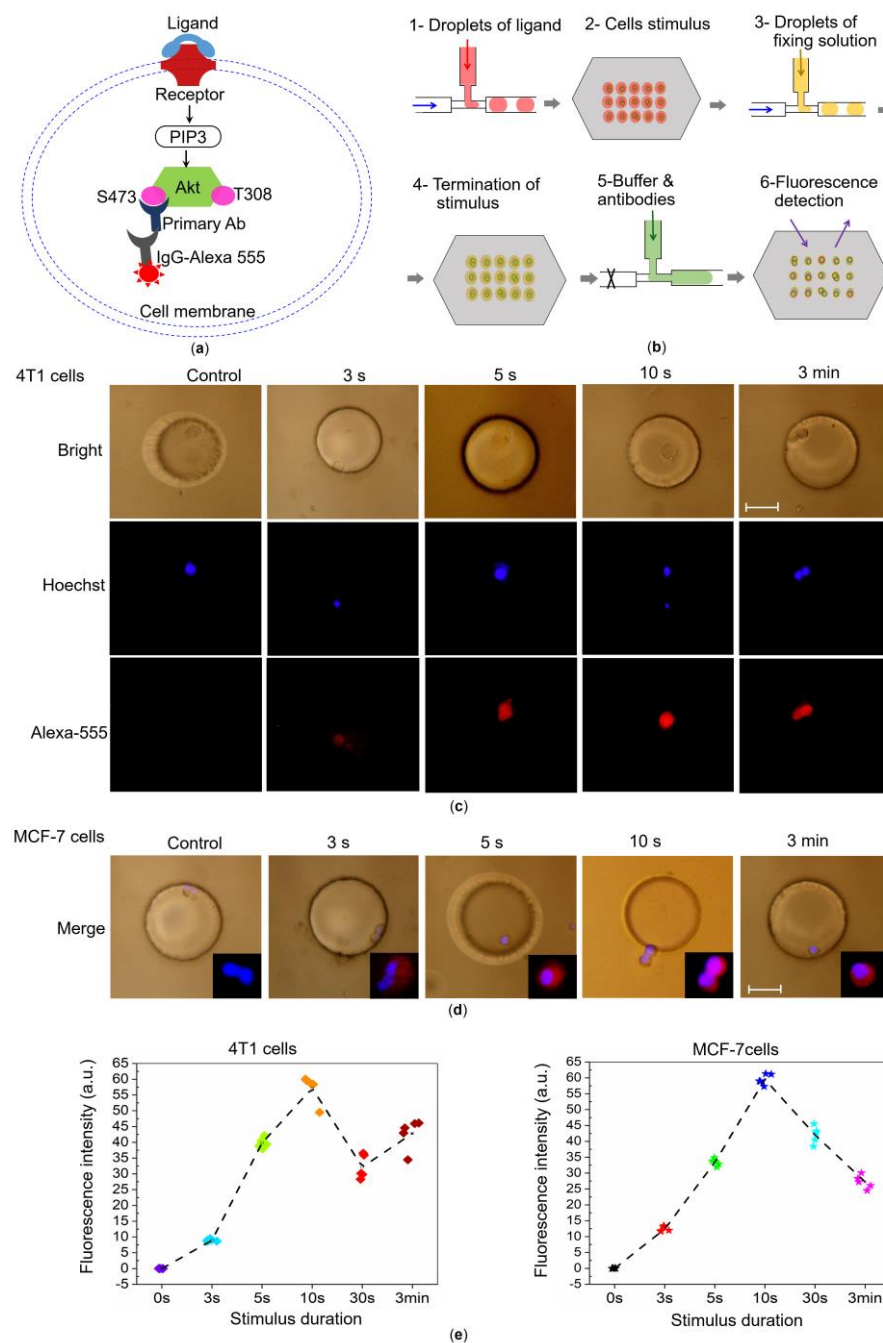
Figure 5. Intracellular protein phosphorylation in the PDGFR/PI3K/Akt pathway induced by PDGF-BB stimulation. (**a**) Schematic diagram illustrating the signal transduction pathway. (**b**) Schematic diagram depicting single-cell treatment with the ligand and sequential immunocytochemistry steps for probing protein phosphorylation. (**c**) 4T1 single cells were stimulated with PDGF-BB droplets for varying time periods, followed by replacement with fixing droplets. Representative pictures of the 4T1 cells under a SEW after the procedure: bright-field row: single cells remained intact and adherent; Hoechst row: blue fluorescence was used for cell localization and validation; Alexa-555 row: the obtained red fluorescence intensities correspond to phosphorylation levels. (**d**) MCF-7 single cells were subjected to the same immunocytochemistry steps. (**e**) The fluorescence intensities of five single cells measured at each stimulus duration; the mean values are connected with a dashed line. Scale bars: 50 μm.

As expected, the individual cells in the control group without PDGF-BB stimulus did not exhibit receptor phosphorylation, as evidenced by the Hoechst(+) and Alex-55(−)

fluorescence intensities shown in Figure 5c. Increasing the stimulation time to 3 s resulted in the phosphorylation of PDGFR being triggered on the cell membrane, resulting in low phosphorylation levels, as indicated by the weak red fluorescence in the second column of Figure 5c. With a prolonged stimulation of 5 s, the red fluorescence of individual cells was significantly enhanced, indicating a higher abundance of phosphorylated states. With prolonged stimulation to 10 s, the red fluorescence of individual cells continued to be enhanced, indicating a sustained increase in phosphorylation level. In a long-term control trial, the red fluorescence of single cells stimulated for 3 min did not change significantly compared to that at 5 s, indicating that complete phosphorylation was achieved at approximately 5 s; the response at the bulk or average level was detected using flow cytometry (Figure S7). In addition, to prove the versatility of the SEW-based platform, MCF-7 cells underwent the same protocol, with the exception of the Anti-Akt primary antibody for Ser473 recognition, and similar phosphorylation results were obtained after 3 s, 5 s, 10 s and 3 min of stimulus, as shown in Figure 5d. Figure 5e shows the fluorescence intensities of the secondary antibody for five single cells measured at each stimulus duration, and the mean values are connected with a dashed line. These results suggest that receptor phosphorylation of PDGFR may be triggered within 3 s of ligand stimulation with PDGF-BB and completed within only 10 s of stimulus time. Gaining insights into single-cell responses to transient stimuli has not been feasible using traditional methods. Specifically, the result of cell phosphorylation being completed within only 10 s of stimulus time is also found within the previous literature report [23]. However, the initiation time of receptor phosphorylation of PDGFR in a stimulated cell is as fast as 3 s, which to our knowledge is the first time that this has been observed. Moreover, to evaluate the effects of the shear stress during droplet replacement on the signaling pathway [40], Akt phosphorylation of MCF-7 cells was also observed under 'extreme' conditions, whereby culture medium droplets containing the inhibitor were trapped and replaced across single cells 240 times during 1 min. Figure S8 shows that the phosphorylation response of cells treated in this manner did not differ significantly from that of undisturbed cells, which further suggests that the SEW-based strategy did not alter the signaling pathway. We propose that the SEW-based platform may be an important new technique for probing temporal dynamics of fast cellular events at a single-cell level for a wide range of applications.

4. Conclusions

In conclusion, with the aim of realizing droplet trapping and replacement using an SEW structure, we have successfully constructed a multifunction droplet-based microfluidic platform that allows for droplet manipulation, single cell patterning and high spatiotemporal resolved profiling of signaling in a single chip. The SEWs located on the roof of the chamber not only enable droplet replacement with high spatiotemporal resolution, but also near-complete exchange of reagent droplets. Furthermore, single-cell patterning was reliably obtained on the floor of the chamber by harnessing the hydrodynamic flow differences in the SEW region. Moreover, the ability to treat cells using trapped droplets as described for the designed platform, would facilitate subsequent single-cell analysis according to the immunohistochemistry protocol. Considering such advantages, the SEW-based device was applied to analyze the phosphorylation states of PDGFR and the downstream signaling protein Akt, and evaluate the effects of time-dependent stimuli on tumor cells. The present study provides a general platform for investigating the temporal dynamics of signal profiling at the single-cell level, based on adherent cell manipulation. Furthermore, the new strategy also has significant potential for rapid chemical reaction monitoring for a wide range of applications.

Supplementary Materials: The following supporting information can be downloaded at: https://www.mdpi.com/article/10.3390/chemosensors10120521/s1, Supplementary figures including chip dimensions, passing and parking modes, critical volume, time resolution calculated using varying frame rates, cell culture in droplets, cell staining with droplets, flow cytometry results and the control test results involving continuous replacement.

References

1. Lamanna, J.; Scott, E.Y.; Edwards, H.S.; Chamberlain, M.D.; Dryden, M.D.M.; Peng, J.; Mair, B.; Lee, A.; Chan, C.; Sklavounos, A.A.; et al. Digital microfluidic isolation of single cells for -Omics. *Nat. Commun.* **2020**, *11*, 5632–5644. [CrossRef]
2. Tay, S.; Hughey, J.J.; Lee, T.K.; Lipniacki, T.; Quake, S.R.; Covert, M.W. Single-cell NF-(kgr)B dynamics reveal digital activation and analogue information processing. *Nature* **2010**, *466*, 267–271. [CrossRef] [PubMed]
3. Kamenz, J.; Ferrell, J.E. The Temporal Ordering of Cell-Cycle Phosphorylation. *Mol. Cell* **2017**, *65*, 371–373. [CrossRef] [PubMed]
4. Aibar, S.; González-Blas, C.B.; Moerman, T.; Huynh-Thu, V.A.; Imrichova, H.; Hulselmans, G.; Rambow, F.; Marine, J.-C.; Geurts, P.; Aerts, J.; et al. SCENIC: Single-cell regulatory network inference and clustering. *Nat. Methods* **2017**, *14*, 1083–1086. [CrossRef]
5. Bedard, P.L.; Hansen, A.R.; Ratain, M.J.; Siu, L.L. Tumour heterogeneity in the clinic. *Nature* **2013**, *501*, 355–364. [CrossRef] [PubMed]
6. Peng, A.; Mao, X.; Zhong, J.; Fan, S.; Hu, Y. Single-cell multi-Omics and its prospective application in cancer biology. *Proteomics* **2020**, *20*, 1900271–1900279. [CrossRef]
7. Clark, I.C.; Delley, C.L.; Sun, C.; Thakur, R.; Stott, S.L.; Thaploo, S.; Li, Z.; Quintana, F.J.; Abate, A.R. Targeted single-cell RNA and DNA sequencing wth fluorescence activated droplet merger. *Anal. Chem.* **2020**, *92*, 14616–14623. [CrossRef]
8. Du, L.; Liu, H.; Zhou, J. Picoliter droplet array based on bioinspired microholes for in situ single-cell analysis. *Microsystems Nanoeng.* **2020**, *6*, 33–41. [CrossRef]
9. Tajik, M.; Baharfar, M.; Donald, W.A. Single-cell mass spectrometry. *Trends Biotechnol.* **2022**, *40*, 2182–2200. [CrossRef]
10. Bendall, S.C.; Nolan, G.P.; Roederer, M.; Chattopadhyay, P.K. A deep profiler's guide to cytometry. *Trends Immunol.* **2012**, *33*, 323–332. [CrossRef]
11. Krutzik, P.O.; Crane, J.M.; Clutter, M.R.; Nolan, G.P. High-content single-cell drug screening with phosphor specific flow cytometry. *Nat. Chem. Biol.* **2008**, *4*, 132–142. [CrossRef] [PubMed]
12. Junkin, M.; Kaestli, A.J.; Cheng, Z.; Jordi, C.; Albayrak, C.; Hoffmann, A.; Tay, S. High-Content Quantification of Single-Cell Immune Dynamics. *Cell Rep.* **2016**, *15*, 411–422. [CrossRef]
13. Samlali, K.; Ahmadi, F.; Quach AB, V.; Soffer, G.; Shih, S.C.C. One cell, one drop, one click: Hybrid microfluidics for mammalian single cell isolation. *Small* **2020**, *16*, 2002400–2002412. [CrossRef] [PubMed]
14. Zhang, K.; Chou, C.-K.; Xia, X.; Hung, M.-C.; Qin, L. Block-Cell-Printing for live single-cell printing. *Proc. Natl. Acad. Sci. USA* **2014**, *111*, 2948–2953. [CrossRef]
15. Brimmo, A.T.; Menachery, A.; Sukumar, P.; Qasaimeh, M.A. Noncontact Multiphysics Probe for Spatiotemporal Resolved Single-Cell Manipulation and Analyses. *Small* **2021**, *17*, 2100801. [CrossRef]
16. Tanay, A.; Regev, A. Scaling single-cell genomics from phenomenology to mechanism. *Nature* **2017**, *541*, 331–338. [CrossRef] [PubMed]
17. Mann, M.; Jensen, O.N. Proteomic analysis of post-translational modifications. *Nat. Biotechnol.* **2003**, *21*, 255–261. [CrossRef]
18. Lou, Q.; Ma, Y.; Zhao, S.-P.; Du, G.-S.; Fang, Q. A flexible and cost-effective manual droplet operation platform for miniaturized cell assays and single cell analysis. *Talanta* **2020**, *224*, 121874–121882. [CrossRef]
19. Xie, R.; Liu, Y.; Wang, S.; Shi, X.; Zhao, Z.; Liu, L.; Liu, Y.; Li, Z. Combinatorial perturbation sequencing on single cells using microwell-based droplet random pairing. *Biosens. Bioelectron.* **2023**, *220*, 114913–114921. [CrossRef]

20. Blazek, M.; Santisteban, T.S.; Zengerle, R.; Meier, M. Analysis of fast protein phosphorylation kinetics in single cells on a microfluidic chip. *Lab Chip* **2014**, *15*, 726–734. [CrossRef]

21. Ng, A.; Chamberlain, M.; Situ, H.; Lee, V.; Wheeler, A.R. Digital microfluidic immunocytochemistry in single cells. *Nat. Commun.* **2015**, *6*, 7513–7524. [CrossRef]

22. Ying, Y.-L.; Hu, Y.-X.; Gao, R.; Yu, R.-J.; Gu, Z.; Lee, L.P.; Long, Y.-T. Asymmetric Nanopore Electrode-Based Amplification for Electron Transfer Imaging in Live Cells. *J. Am. Chem. Soc.* **2018**, *140*, 5385–5392. [CrossRef] [PubMed]

23. Yu, R.; Ying, Y.; Gao, R.; Long, Y. Confined Nanopipette Sensing: From Single Molecules, Single Nanoparticles, to Single Cells. *Angew. Chem. Int. Ed.* **2019**, *58*, 3706–3714. [CrossRef] [PubMed]

24. Guillaume-Gentil, O.; Grindberg, R.V.; Kooger, R.; Dorwling-Carter, L.; Martinez, V.; Ossola, D.; Pilhofer, M.; Zambelli, T.; Vorholt, J.A. Tunable Single-Cell Extraction for Molecular Analyses. *Cell* **2016**, *166*, 506–516. [CrossRef]

25. Guillaume-Gentil, O.; Potthoff, E.; Ossola, D.; Franz, C.M.; Zambelli, T.; Vorholt, J.A. Force-controlled manipulation of single cells: From AFM to FluidFM. *Trends Biotechnol.* **2014**, *32*, 381–388. [CrossRef]

26. Sarkar, A.; Kolitz, S.; Lauffenburger, D.A.; Han, J. Microfluidic probe for single-cell analysis in adherent tissue culture. *Nat. Commun.* **2014**, *5*, 3421. [CrossRef]

27. Dangla, R.; Lee, S.; Baroud, C.N. Trapping Microfluidic Drops in Wells of Surface Energy. *Phys. Rev. Lett.* **2011**, *107*, 124501. [CrossRef]

28. Fradet, E.; McDougall, C.; Abbyad, P.; Dangla, R.; McGloin, D.; Baroud, C.N. Combining rails and anchors with laser forcing for selective manipulation within 2D droplet arrays. *Lab Chip* **2011**, *11*, 4228–4234. [CrossRef]

29. Hele-Shaw, H. Flow of water. *Nature* **1898**, *58*, 520. [CrossRef]

30. Abbyad, P.; Dangla, R.; Alexandrou, A.; Baroud, C.N. Rails and anchors: Guiding and trapping droplet microreactors in two dimensions. *Lab Chip* **2010**, *11*, 813–821. [CrossRef]

31. Sart, S.; Tomasi, R.F.-X.; Amselem, G.; Baroud, C.N. Multiscale cytometry and regulation of 3D cell cultures on a chip. *Nat. Commun.* **2017**, *8*, 469–481. [CrossRef]

32. Lin, M.; Mao, S.; Wang, J.; Xing, J.; Wang, Y.; Cai, K.; Luo, Y. Adsorption force of fibronectin controls transmission of cell traction force and subsequent stem cell fate. *Biomaterials* **2018**, *162*, 170–182. [CrossRef]

33. Herrada, M.; Ponce-Torres, A.; Rubio, M.; Eggers, J.; Montanero, J. Stability and tip streaming of a surfactant-loaded drop in an extensional flow. Influence of surface viscosity. *J. Fluid Mech.* **2022**, *934*, A26–A37. [CrossRef]

34. Sousa, A.M.; Pereira, M.J.; Matos, H.A. Oil-in-water and water-in-oil emulsions formation and demulsification. *J. Pet. Sci. Eng.* **2022**, *210*, 110041–110058. [CrossRef]

35. Basciani, S.; Mariani, S.; Spera, G.; Gnessi, L. Role of platelet-derived growth factors in physiology and medicine. *Genes Dev.* **2008**, *22*, 1276–1312.

36. Yudushkin, I. Control of Akt activity and substrate phosphorylation in cells. *IUBMB Life* **2020**, *72*, 1115–1125. [CrossRef] [PubMed]

37. Yua, C.; Suna, P.; Zhoua, Y.; Shena, B.; Zhoua, M.; Wua, L.; Kong, M. Inhibition of AKT enhances the anti-cancer effects of Artemisinin in clear cell renal cell carcinoma. *Biomed. Pharmacother.* **2019**, *118*, 109383–1092391. [CrossRef]

38. Lemmon, M.A.; Schlessinger, J. Cell Signaling by Receptor Tyrosine Kinases. *Cell* **2010**, *141*, 1117–1134. [CrossRef]

39. Manning, B.D.; Cantley, L.C. AKT/PKB Signaling: Navigating Downstream. *Cell* **2007**, *129*, 1261–1274. [CrossRef]

40. Lee, S.; Gallaire, F.; Baroud, C.N. Interface-induced recirculation within a stationary microfluidic drop. *Soft Matter* **2012**, *8*, 10750–10758. [CrossRef]